IEEE Access
Multidisciplinary | Rapid Review | Open Access Journal

SPECIAL SECTION ON DATA-ENABLED INTELLIGENCE FOR DIGITAL HEALTH

Received November 11, 2019, accepted November 22, 2019, date of publication November 25, 2019,
date of current version December 10, 2019.

Digital Object Identifier 10.1109/ACCESS.2019.2955710

Extraction Method of Coronary Artery Blood Vessel Centerline in CT Coronary Angiography

XIAODONG SHENG, TAO FAN, XIAOQI JIN, JING JIN, ZHIXIAN CHEN, GUANQUN ZHENG, MIN LU, AND ZONGCHENG ZHU

Changshu No.2 People's Hospital, Changshu 215500, China

Corresponding author: Tao Fan (shengxiaodong_cs@163.com)

This work was supported in part by the Jiangsu Committee of Health under Grant H2018071, in part by the National Natural Science Foundation of China under Grant 61702225, Grant 61772241, and Grant 61902152, in part by the Natural Science Foundation of Jiangsu Province under Grant BK20180600, and in part by the Science and Technology Demonstration Project for Social Development of Wuxi under Grant WX18IVJN002.

ABSTRACT Aiming at the problem that the traditional coronary artery centerline extraction method is computationally intensive and requires a large number of manual interventions, a fully automatic coronary artery centerline tracking extraction method is proposed. First, adaptive adaptation of coronary vessels was performed based on different Fresenius norms designed for coronary scale. A multi-scale differential operator is constructed based on the vascular gray-scale distribution to establish a discriminant function, thereby obtaining the initial position and tracking direction of the seed point. Then, the new ridge point and tracking direction are optimally detected within the local arc length of the initial direction to ensure that the correct ridge position can still be obtained with large error interference. Finally, the pseudo vascular centerline is removed using the vascular topology feature detection method. The experimental results show that the method can accurately extract the blood vessel center line, direction vector and other information in the coronary angiography image without manual intervention, and can be used in the computer-assisted diagnosis and treatment process of clinical cardiovascular disease.

INDEX TERMS Extraction method, coronary artery blood, vessel Centerline, CT coronary angiography.

I. INTRODUCTION

CT coronary angiography is a new minimally invasive angiography technique that combines spiral CT scanning with computerized three-dimensional imaging reconstruction techniques [1], [2]. With the development and improvement of CT equipment, its scanning speed and spatial resolution have been greatly improved, thereby improving image quality. In addition, reports on the use of coronary CTA in the clinical diagnosis of cardiovascular and cerebrovascular diseases are increasing. Detection, segmentation, and visualization of blood vessels in coronary CTA images can be of great help to physicians in diagnosing cardiovascular and cerebrovascular diseases. According to the latest domestic survey report, 3 million of the deaths in China each year have died of cardiovascular and cerebrovascular diseases, accounting for about 40% of all deaths of the national population. It is the number one killer of Chinese residents [3]. Therefore, early quantitative diagnosis and risk assessment of cardiovascular and cerebrovascular diseases is very important to prolong human life expectancy and improve the quality of life of human beings. In clinical diagnosis and treatment, doctors often need to analyze and judge the angiographic image of the patient [4]. Among them, the central line extraction of coronary artery is the most important and most important part of blood vessel segmentation [5].

Coronary angiography is an important means of clinical diagnosis. Quantitative analysis of coronary arteries has important practical significance. Compared with traditional qualitative diagnosis methods, it overcomes the subjective randomness of doctors' judgment and provides a more objective and accurate diagnosis basis. Automated extraction of coronary artery contours and centerline is a prerequisite for quantitative analysis of coronary arteries. In coronary angiography images, coronary artery vascular extraction can be based on region or edge based image segmentation techniques. Robertson *et al.* [6] pointed out that the grayscale distribution of coronary artery vessels is

The associate editor coordinating the review of this manuscript and approving it for publication was Yongtao Hao.

approximately Gaussian, so the two-dimensional Gaussian template is used to extract coronary artery vessels, but this method is time consuming. Tagliari *et al.* [7] replaced the two-dimensional Gaussian template with a one-dimensional rotating Gaussian template, which reduced the complexity of the algorithm. However, from the perspective of accurate analysis, accurate extraction of coronary artery vascular margins in coronary artery vascular analysis is a better choice. In many existing coronary artery contour extraction algorithms, the detection of coronary artery centerline is the most critical and difficult step. The easiest way is to draw [8] by hand, but this method is time-consuming and laborious and has poor repeatability, so it is gradually replaced by a semi-automatic method of human-computer interaction. In these interactive methods, the operator only needs to specify the starting point and ending point of the coronary artery segment to be analyzed, and the center line between the two points can be automatically obtained [9].

The existing centerline extraction algorithms are mostly based on dynamic programming methods, and the search time is long, which is difficult to meet the requirements of clinical real-time. Due to the complex structure of coronary arteries, and the influence of contrast agent on imaging, the gray scale distribution of images tends to be uneven, which makes it difficult to extract the centerline of coronary artery vessels [10], [11]. Coronary artery the centerline of the vessel appears as a ridgeline composed of a series of ridge points. The ridge point is the local extremum of the image brightness in a certain direction, and it appears as the gray extreme value of the vertical blood vessel in the coronary artery image. Pudov and Dragoshanskii [12] used the gradient of the image and the Hessian matrix to give the definition of the ridge point. Breitenreicher *et al.* [13] listed the expressions of Hessian matrices at ridge points under three ideal vascular model conditions. In the actual medical images obtained, due to the influence of the dose and distribution of the contrast agent, the gray distribution characteristics of the blood vessels cannot fully conform to the above characteristics, so the centerline of the blood vessels cannot be described by the nature of the ridge points. Bayat *et al.* [14] used Hessian matrix to analyze the characteristics of blood vessels, established a series of vascular discriminant criteria, and formed a discriminant function by discriminant criteria, and obtained a multiscale vessel enhancement filtering (MVEF). The MVEF can be effectively enhanced along the centerline of the blood vessel, and the closer to the centerline, the more enhanced it is, highlighting the characteristics of the ridgeline of the vessel centerline. However, in the process of extracting the ridge points of the image, it was found that when the blood vessel was enhanced by MVEF, the large-sized blood vessel portion was enhanced, and the ridge point was easily extracted. However, the effect of small-sized blood vessels is not obvious, and it is not easy to extract the ridge points. Cao *et al.* [15] needed to initiate vascular tracking by labeling some of the seed points in the blood vessel. When using the snake algorithm for image segmentation, it is also necessary to set the seed point to iteratively extract the boundary. However, this way of manually extracting seed points seriously affects the consistency of the algorithm, and brings uncertain human factors to the extracted results. Shrichandran *et al.* [16] summarized a multi-scale vascular ridge point discriminant function by analyzing three basic vascular models, and found the position of the ridge point when the function obtained the extremum. Rajan and Kavitha [17] designed a multi-scale ridge determination function based on the angular relationship between the characteristic direction of the Hessian matrix at the pixel and the pixel gradient, and realized the extraction of the coronary artery centerline in the fundus retina image. Alam *et al.* [18] extracted the centerline of the coronary artery by tracking the ridge point in the multi-scale space of the image by defining the initial seed point. However, the choice of scale is a problem. If the sampling interval of the scale is too large, the result cannot be accurately obtained; on the contrary, a large number of complicated convolution calculations are added, which seriously affects the efficiency of the algorithm.

This paper designs a method for tracking ridge points for extracting the centerline of coronary arteries. First, adaptive adaptation of coronary vessels was performed based on different Fresenius norms designed for coronary scale. A multi-scale differential operator is constructed based on the vascular gray-scale distribution to establish a discriminant function, thereby obtaining the initial position and tracking direction of the seed point. Then, the new ridge point and tracking direction are optimally detected within the local arc length of the initial direction to ensure that the correct ridge position can still be obtained with large error interference. Finally, the pseudo vascular centerline is removed using the vascular topology feature detection method.

The rest of our paper was organized as follows. Related basic knowledge was introduced in Section. II. Extraction of coronary artery centerline was introduced in Section. III. Experimental results and analysis were discussed in detail in Section. IV. Finally, Section. V concluded the whole paper.

II. RELATED BASIC KNOWLEDGE

A. CORONARY ANGIOGRAPHY

With the development of modern technology, it has been known that radiation is not easily transmitted through a contrast agent containing a high concentration of iodine solution. The contrast agent is injected into the blood vessels of the heart through a special catheter with a high-pressure syringe. When the contrast agent passes through the heart or blood vessels with the blood, a series of angiograms are taken with a fast camera, and the cardiovascular internal structure and blood can be directly obtained. Information on flow conditions, this is ray coronary angiography [19].

Angiography can be divided into conventional angiography and selective angiography. For example, the left ventricle and the right ventricle and the aorta belong to the former, and coronary angiography belongs to the latter.

1) CONVENTIONAL ANGIOGRAPHY

Right ventricular angiography is a right ventricular intubation through the femoral vein, rapid injection of contrast agents, showing the right heart chamber and pulmonary vessels for the observation of right heart, pulmonary blood vessels, and congenital heart disease.

Left ventricular angiography is the insertion of a catheter through the peripheral artery into the left ventricle followed by injection of a contrast agent. For mitral insufficiency, aortic stenosis, ventricular septal defect, permanent compartment common and left ventricular lesions.

Aortography is the insertion of the catheter through the percutaneous artery. The tip of the catheter is usually placed on the aortic valve, and the upper part of the ascending aorta, aortic arch and descending aorta can be developed. Suitable for showing lesions in the aorta itself, aortic insufficiency, abnormal communication between the aorta and the pulmonary artery or the aorta and the right heart.

2) SELECTIVE ANGIOGRAPHY

Selective angiography is the direct and rapid injection of contrast agent into the selected cardiac cavity or great vessels with the aid of catheter, so that the highest concentration can be achieved quickly and the lesions in the region can be clearly demonstrated. At present, it has become one of the commonly used methods of diagnosis of vascular diseases, especially for complicated cardiovascular malformations and coronary artery bypass surgery diagnosis is essential. Selective right heart angiography, left heart angiography, pulmonary artery angiography, aortic angiography, coronary angiography and hepatic artery, renal artery, cerebrovascular, celiac artery, mesenteric artery angiography are commonly used.

Coronary angiography began in 1933 [20]. Currently, special cardiac catheters with curved tips can be used to enter the left and right coronary orifice respectively and inject contrast agent to develop the left and right coronary arteries separately. In clinical application, multiple injection and multi-angle projection are allowed, which can obviously improve the diagnostic effect.

Digital subtraction angiography (DCG) is a computer-assisted angiography method, also known as digital angiography. It is a new radiographic technique applied in clinic since last century. It is to use the computer to improve the blood vessel image with low iodine concentration to the level visible to the naked eye, and eliminate the tissue image other than angiographic vessels, so as to facilitate the study of vascular diseases or other diseases caused by abnormalities.

Figure 1 shows the basic structure of the traditional c-arm radiographic contrast machine. During the operation, film and TV images are used for dynamic observation, and video is obtained by tape recording device, which is repeatedly played on the monitor screen to assist the doctor in diagnosis of the disease. Nowadays, image digitization has become an important part of medical modernization. Digital images

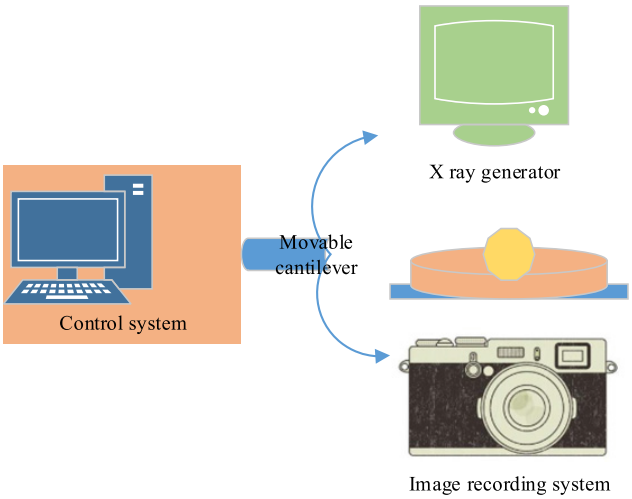

FIGURE 1. Schematic diagram of coronary angiography equipment.

can be obtained by adding TV camera system and module conversion system after traditional X-ray machine.

Coronary angiography system can be divided into two types: double-sided angiography system and single-sided angiography system. The duplex imaging system has two sets of X-ray imaging devices that simultaneously image the coronary arteries from two different angles to obtain two still coronary angiogram images or image sequences. A monangiography system consists of only one set of X-ray imaging devices that, at one point in time, take an image of a coronary artery from an angle, producing a still image or sequence of images.

As can be seen from the working process of the double-sided contrast angiography system and the single-sided contrast angiography system, the biggest difference between the two systems is that the former can obtain the contrast angiography images from two different angles at one time while the latter can only obtain the contrast angiography images from one angle at one time. Although double-sided imaging system for 3D reconstruction of coronary artery has brought great convenience, but at present, the clinical application of double coronary angiography system is not too much, the reason mainly has the following two aspects: one is the double imaging system restricts the medical staff of space operation, clinical operation is not very convenient second, double-sided imaging system's cost is relatively high. From the perspective of application prospect, it is of better research value and clinical significance to choose two different angles of single-sided coronary angiography images to reconstruct three-dimensional coronary arteries.

B. CHARACTERISTICS OF CORONARY ANGIOGRAPHY

In order to reduce the harm of X-ray to patients and doctors, only 25 angiograms are taken in one cardiac cycle. During angiography, patients were asked to hold their breath to reduce the impact of respiratory movement. Electrocardiogram signals were recorded synchronously. Then, according

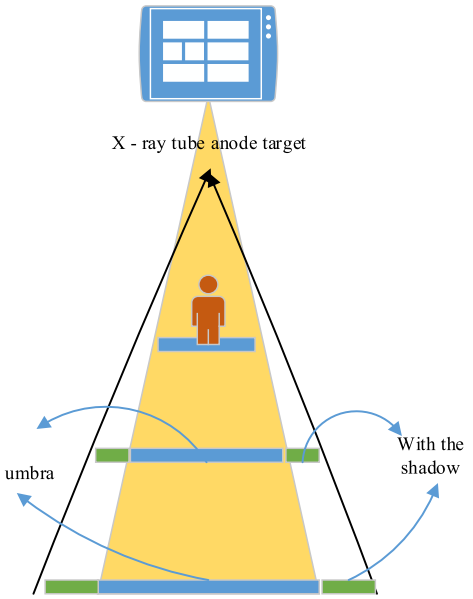

FIGURE 2. A conical projection of an X-ray.

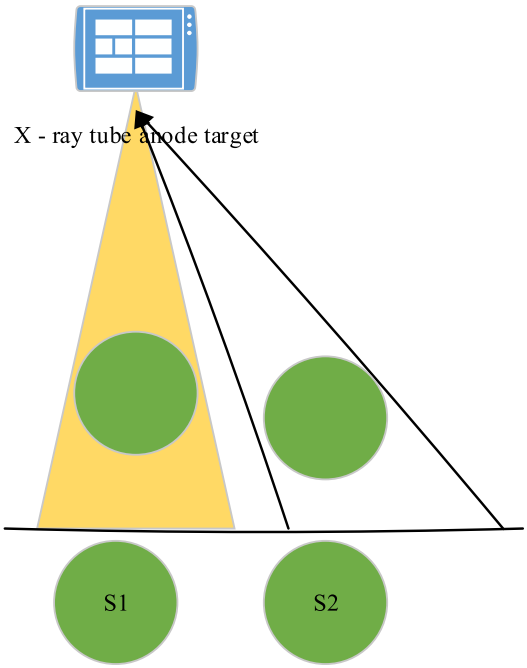

FIGURE 3. Image distortion caused by X-ray conical projection.

to the electrocardiogram signals, angiogram images were selected at the same time in the cardiac cycle.

The X-ray source of the imaging system is a source close to the point but with a certain area. A cone-shaped ray beam is emitted by the X-ray source to make a cone-shaped projection on the target object, so the image is amplified to a certain extent and shadow is generated, as shown in Figure 2, which reduces the sharpness of the image. In addition, the conical projection of X-ray may also lead to image distortion. As shown in Figure 3, the same size sphere was projected on the central axis and edge of the X-ray beam, respectively, resulting in projected images S1 and S2. Obviously, both of them were amplified, but the image S2 was distorted due to oblique projection. Therefore, the edge of the contrast image not only has shadowing and poor sharpness, but also has geometric distortion caused by the oblique projection of X-ray [21].

Three-dimensional human tissue structures were accumulated along the direction of the ray and superimposed on the imaging image plane to obtain a two-dimensional projection. Radiographic images typically contain structures such as blood vessels, soft tissues and bones, but in the diagnosis of vascular disease it is desirable to highlight the structures of blood vessels and remove images of surrounding tissue. Due to the uneven distribution of contrast agent and projection of spine and other tissues, the image contrast is poor and the gray distribution is uneven, which increases the difficulty of clinical observation and treatment.

Coronary angiography images are strong noise images with low signal-to-noise ratio, mainly including salt, and pepper noise, random noise, and structural noise [22]. Noise pollution sources mainly include the following aspects:

(1) The non-uniformity of X-ray exposure will introduce some noise and reduce the image contrast.

(2) The gray value of angiographic images not only changes along different locations of blood vessels, but also is related to the distance of X-ray sources and the density of contrast agents. Gray values of the same blood vessel can also change in different images.

(3) The projection of human soft tissues and bones may also change the background structure of vascular projection area, for example, the projection of ribs will reduce the contrast of some areas of the image.

(4) Some tissues, such as the shape of the catheter used for angiography, are similar to the blood vessel, forming structural noise, which increases the difficulty of automatic identification of blood vessel.

C. CLASSIFICATION OF CORONARY ARTERY CENTERLINE EXTRACTION METHODS

So far, many methods have been proposed for coronary artery centerline extraction. The simplest centerline extraction method is the manual extraction method, which is to manually mark the location of the center points along the coronary arteries in a monolayer or three-dimensional image and finally connect these center points. Although the method is accurate, it is time-consuming and laborious. Therefore, automatic or semi-automatic extraction method is necessary. Automatic or semi-automatic centerline extraction methods can be classified into five categories: topology-based refinement, range-based transformation, path-based planning, track-based and various other centerline extraction methods.

1) METHOD BASED ON TOPOLOGY REFINEMENT

The method based on topological refinement [23], [24] is to continuously remove the outer layer of coronary artery

vessels by using morphological decay candle operation until only the skeleton of the vessel is left. To prevent excessive refinement of blood vessels, deletion of vascular endpoints should be avoided. Only boundary voxels that do not affect connectivity and topology after deletion can be deleted. There are many three-dimensional refinement methods that only extract the axial surface of coronary arteries and then use other algorithms to obtain the center curve from the axial surface.

A centerline extracted based on a refinement method may contain incorrect branching, so the method typically involves two steps. First, the coronary arteries are refined, resulting in a rough centerline with a unit-element width. Then, cross the centerline to remove the wrong loops, branches, and gaps, ensuring that there is only a single, complete centerline between the starting point and the end point.

The method based on refinement has two kinds of algorithms: serial computation and parallel computation. Serial computation can delete only one point in each iteration, while parallel computation can delete several points at the same time. Topological refinement method can well maintain the topological structure and connectivity of coronary arteries and has a high accuracy. However, as it is an iterative process, it is time-consuming and more susceptible to image quality.

2) METHOD BASED ON DISTANCE TRANSFORMATION

Distance transformation based method [25], [26] is a popular method to extract the center line. This method determines the centerline by locating the group of points farthest from the coronary artery boundary. Approximate Euclidean distance is usually used in the discrete domain. The distance transformation of voxel points with respect to the boundary was used to determine the maximum endovascular sphere of the coronary artery. The largest endovascular sphere is a sphere with the largest radius inside the coronary artery composed of a series of connected voxels. The sphere is completely contained within the coronary artery, but is not contained within the sphere of any other coronary artery. The center of this series of largest incised spheres forms the centerline of the coronary artery. The distance-graph-based approach specifies that each point inside the coronary artery has a distance value that is the minimum distance from the point to the boundary. The centerline of the coronary artery is then obtained by connecting the local maximum in the distance diagram.

Among the many centerline extraction methods based on distance transformation, the method proposed by Jang and Hong [27] is one of the most representative. This method uses two kinds of distance transformation simultaneously, one is the traditional distance transformation based on boundary, and the other is the distance transformation based on seed points. The seed point distance transformation is used to determine the equidistant line relative to the seed point and to determine the end points of each branch based on this information. Then a preliminary centerline is obtained by sequentially connecting the maximum boundary distance points of each isometric line. Finally, the accurate centerline is obtained through post-processing steps.

3) PATH PLANNING-BASED APPROACH

Path planning-based method [28], [29] is another kind of centerline extraction technology. The main idea of this method is to first select an initial path along the blood vessel that connects two given points. The pathway is then adjusted until it is in the center of the blood vessel. When a blood vessel has multiple branches, a reference point is usually selected and the endpoints of each branch are connected to the reference point to obtain the initial path, which is usually determined according to the shortest path principle.

4) TRACEABILITY BASED METHOD

The tracing method [30], [31] obtained the approximate center-line trend of the current position by judging the local direction of coronary arteries, and obtained the center point of the cross section of coronary arteries at the current position by combining the local information of the vessels in the image. Then, according to the obtained center point, the direction of the center line was corrected, and the above calculation process of local center point was repeated until the end of the coronary artery was traced. The method based on tracking is simple to implement, short time, and can solve the continuity problem of center line. However, because this method is based on the local method and global information is not considered in the tracking process, sometimes the obtained centerline will be incomplete. Moreover, because this method is not sensitive to the overall topological structure of coronary arteries, it is easy to make mistakes in the extraction of centerline when the curvature changes greatly or branches are more.

In this paper, with the help of the above references, image preprocessing, seed point selection and tracking direction of vessel centerline were improved, and a method of tracking ridge points was designed to extract the centerline of coronary artery, realizing the automatic acquisition of vessel centerline.

III. EXTRACTION METHOD OF CORONARY ARTERY CENTERLINE

A. ADAPTIVE VASCULAR ENHANCEMENT

In the process of using ridge points to extract the centerline of blood vessels, it is necessary to ensure that the centerline of blood vessels is the brightest or darkest curve in the image. However, the actual image of the blood vessels is often unable to meet this condition. Therefore, it is necessary to strengthen the blood vessels so that the characteristics of the enhanced blood vessels along the central line are more obvious.

MVEF designed a multi-scale response function V based on the characteristics of vascular tubular shape and the eigenvalues of Hessian matrix. Through the filter, the image is enhanced to make the tubular object in the image have the highest gray level along the center line and the gray level is weakened towards the edge, but the non-tubular object

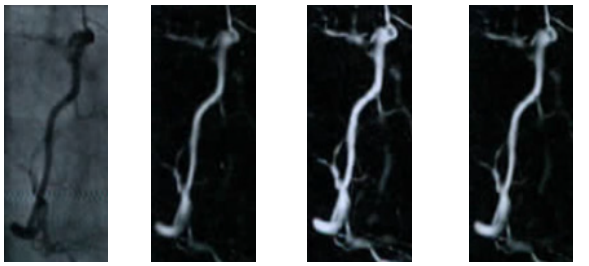

(a) Angiography of blood vessels (b) MVEF enhancement (β=15) (c) MVEF enhancement (β=8) (d) AMVEF enhancement

FIGURE 4. Comparison of vascular enhancement effect.

is darkened. The expression of V is shown in equation (1) and equation (2).

$$V(s) = \begin{cases} 0, & \lambda_1 > 0 \\ e^{-\frac{R_\alpha^2}{2\alpha^2}}(1 - e^{-\frac{S^2}{2\beta^2}}), & else \end{cases} \tag{1}$$

$$V = \max_{s_{\min} \le s \le s_{\max}} V(s) \tag{2}$$

$$R_\alpha = \lambda_2/\lambda_1 \tag{3}$$

$$S = ||H||_F = \sqrt{\lambda_1^2 + \lambda_2^2} \tag{4}$$

In the process of using MVEF to enhance vascular images, it was found that the enhancement effect of large-size vessels was good, and the original structural information was basically not lost. However, the enhancement effect of small-sized vessels is poor, and some vascular structures have been blurred, as shown in Figure 4(b).

In the definition of MVEF, the variable α is the parameter that controls R_α, and the variable beta is the parameter that controls S. In general, $\alpha = 0.5$. Variable beta is the maximum Fresenius norm of Hessian matrix of all pixels in the image, namely equation (5).

$$\beta = ||H||_{\max} = \max_{x,y} \sqrt{\lambda_1^2(x, y) + \lambda_2^2(x, y)} \tag{5}$$

In the blood vessels, the effect of MVEF enhancement was not significant when the α changes were large. However, when the β changes, the enhanced effect changes relatively greatly, and the comparison results are shown in Figure 4(b) and Figure 4(c). It has been observed by observation that when β is decreased, the small-sized blood vessel enhancement effect is better. However, large-sized blood vessels are over-extended, which is not conducive to extracting information from the centerline. Therefore, consideration should be given to how to enhance the enhancement of small-sized blood vessels under conditions that ensure that large-sized blood vessels are not excessively enhanced.

In the image, the two eigenvalues $\lambda_1(x, y)$ and $\lambda_2(x, y)$ of the Hessian matrix reflect the maximum and minimum of the second-order differential in the spatial direction at the (x, y) point [32]. And the relationship between the two is shown in equation (6).

$$|\lambda_1(x, y)| \ge |\lambda_2(x, y)| \tag{6}$$

Compared with large-sized blood vessels, the gray scale change of small-sized blood vessels is more obvious, so the Fresenius norm $||H||_F = \sqrt{\lambda_1^2 + \lambda_2^2}$ of the Hessian matrix of the pixel on the small blood vessels is larger than that of the large blood vessels. Therefore, it is not reasonable for MVEF to use an unchanging β value to construct an enhancement filter suitable for blood vessels of different sizes.

In this paper, the adaptive improvement of MVEF (hereinafter referred to as AMVEF) is based on MVEF, and the β values of different sizes are taken for different sizes of blood vessels. The specific method is to adjust the size of β through $||H||_F$ of the pixel, that is, the equation (7).

$$\beta = f(||H||) = \begin{cases} H_{\max}/2, & H > H_{\max}/2 \\ H_{\max}, & else \end{cases} \tag{7}$$

Through this improvement, the enhancement effect of the small-sized blood vessel is remarkably improved, and the enhancement effect of the large-sized blood vessel is maintained, that is, the structure of the small blood vessel branch is more prominent, as shown in Figure 4(d).

B. TRACKING INITIAL CONDITION

In order to be able to obtain the centerline of the blood vessel by tracking the ridge point, it is necessary to determine the initial position (seed point) for tracking and the initial direction.

1) AUTOMATIC ACQUISITION OF SEED POINTS

In the process of automatically obtaining seed points, based on the enhanced image gray distribution characteristics, the first-order differential information (gradient) and second-order differential information (Hessian matrix) of the image are used to automatically obtain a large number of seeds that can be used for tracking. The main steps are as follows:

Step1. The point of local maximum intensity (PLMI) is detected by combining first-order differential information and second-order differential information near the center line of the blood vessel of the image.

Step2. Finding the seed points on the center line of the corresponding adjacent blood vessels in the direction determined by the first-order differential and the second-order differential at these points, and using these seed points as the initial positions of the tracking.

After the enhancement of blood vessels, the gray level of the pixels along the center line of the blood vessel is locally maximal. According to the definition of spatial extreme points [33], in the gray space of the image, if the pixel point (x, y) is the gray maximum point, then there should be (x, y) = 0, and its Hessian matrix is negative. However, since the points satisfying the above two conditions are not necessarily at the integer coordinate points, a fully automatic PLMI detection method is designed in this paper.

For any pixel point (x, y) and its neighboring pixel points (x + 1, y), (x, y + 1), (x + 1, y + 1); if there is a point (ξ, η) $(x < \xi < x + 1, y < \eta < y + 1)$, such that $(\xi, \eta) = 0$, $\lambda_1(\xi, \eta) < 0$ and $\lambda_2(\xi, \eta) < 0$. The bilinear interpolation

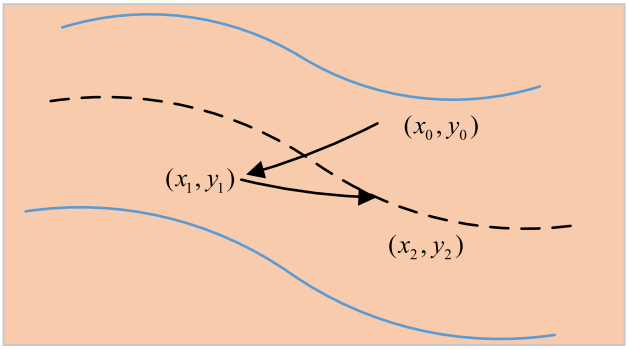

FIGURE 5. Acquisition of PLMI adjacent ridge points.

equation is as shown in equation (8).

$$f(\xi,\eta)=[x+1-\xi x-\xi] \bullet \begin{bmatrix} f(x,y) & f(x,y+1) \\ f(x+1,y) & f(x+1,y+1) \end{bmatrix} \begin{bmatrix} y+1-\eta \\ y-\eta \end{bmatrix} \quad (8)$$

According to the bilinear interpolation equation (8), the necessary and sufficient condition for a point (ξ, η) is a PLMI on the image is solved by equation (9).

$$\begin{cases} (\xi,\eta) = [x+1-\xi x-\xi] \bullet \begin{bmatrix} (x,y)(x,y+1) \\ (x+1,y)(x+1,y+1) \end{bmatrix} \begin{bmatrix} y+1-\eta \\ y-\eta \end{bmatrix} = 0 \\ \lambda_i(\xi,\eta) = [x+1-\xi x-\xi] \bullet \begin{bmatrix} \lambda_i(x,y)\lambda_i(x,y+1) \\ \lambda_i(x+1,y)\lambda_i(x+1,y+1) \end{bmatrix} \begin{bmatrix} y+1-\eta \\ y-\eta \end{bmatrix} < 0 (i=1,2) \end{cases} \quad (9)$$

At this time, the solution (ξ, η) of equation (9) is a PLMI on the image.

This paper chooses (x, y) instead of (ξ, η). On the one hand, precision is not required here, as long as it is inside the blood vessel. On the other hand, the information at (ξ, η) needs to be interpolated from the information of the neighborhood, thus avoiding unnecessary calculations.

After obtaining a large amount of PLMI, it is necessary to find the nearest ridge point on the center line of the blood vessel as the initial position of the tracking. In this process, the paper searches in the direction determined by the first-order differential and the second-order differential (the gradient direction of the image and the feature direction of the Hessian matrix), so that the search process is twice as shown in Figure 5 through the blood vessel center line, ensuring the correctness of the results.

Let (x0, y0) be a PLMI coordinate obtained by the previous process, (x0, y0) be the normalized gradient at (x0, y0), and g1 and g2 are the two components of (x0, y0), respectively. First, look for the gamma maximum point in the (x0, y0) gradient direction, the range is set to d1, and the obtained luminance maximum point is (x1, y1), as shown in the equation (10).

$$I(x_1, y_1) = \max_{0\le d\le d_1} (I(x_0 + g_1 \bullet d, y_0 + g_2 \bullet d)) \quad (10)$$

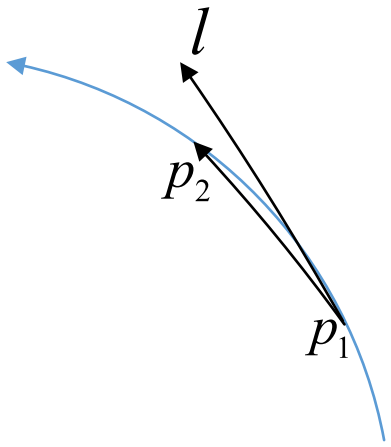

FIGURE 6. Pointing of adjacent ridge points.

Then, in the feature direction corresponding to the eigenvalue with a large absolute value of the Hessian matrix of (x1, y1), the gray maximum point is found, the range is set to d2, and the obtained gray maximum point is (x2, y2), as shown in equation (11).

$$I(x_2, y_2) = \max_{0\le d\le d_2} (I(x_1 + v_{11} \bullet d, y_1 + v_{12} \bullet d)) \quad (11)$$

Let Hessian matrix eigenvalues of (x1, y1) be λ1 and λ2, and $|\lambda_1| \geq |\lambda_2|$, and the corresponding eigenvectors are v1, v2. The variable v11 and the variable v12 are the two components of v1. At this point, (x2, y2) is a seed point.

2) CALCULATION OF INITIAL DIRECTION

The previous analysis in this paper has pointed out that although the characteristic direction of the Hessian matrix can theoretically be used to describe the course of the vessel centerline, there must be errors in the available ridge points and the true ridge points, even if the error is very small, but for the Hessian matrix. The direction of the feature is also very large. Therefore, the direction of the ridge point cannot be simply described by the feature direction of the Hessian matrix.

In Figure 6, if p1, p2 are two adjacent ridge points on the center line. The symbol l is the tangent of the blood vessel centerline at p1, then, according to the definition of the tangent, and $l = \lim_{p_2\to p_1} p_1p_2$. When p1 is close enough to p2, consider using p1 to point p2 in the direction p1p2 instead of tangential l at p1. It is worth noting that, in general, the curvature of the center line of the blood vessel is small, and when the length of p1p2 is small, p1p2 can be approximately equal to l. In addition, the method used to track the ridge points in this paper does not depend entirely on the tracking direction. When there is a small deviation in the tracking direction, the ridge point can still be accurately detected.

According to the above analysis, the method used to determine the initial direction is as follows: first, two adjacent ridge points near the seed point are detected according to the characteristics of the gray scale distribution on the center line of the blood vessel; and then, based on the three points,

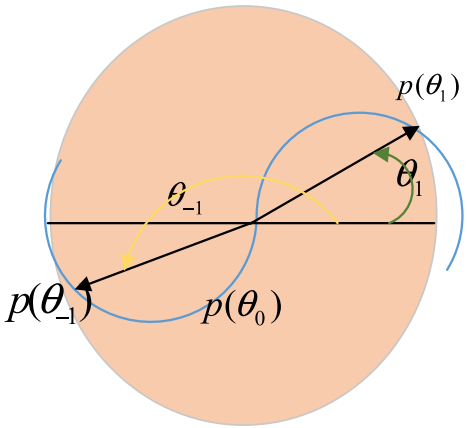

FIGURE 7. Ridge forward and backward initial tracking direction.

the calculation is used for the initial direction of tracking forward and backward.

For any seed point $p(\theta_5)$, if it's coordinate $(x_{\theta_0}, y_{\theta_0})$, as shown in Figure 7, a circle with radius r is made with $p(\theta_0)$ as the center. Thus, the coordinates $p(\theta)$ on the circle can be expressed as equation (12) using the parametric equation.

$$\begin{cases} x = x_{\theta_0} + r \bullet \cos(\theta) \\ y = y_{\theta_0} + r \bullet \sin(\theta), \end{cases} \quad 0 \le \theta \le \pi \tag{12}$$

Since the circle and the blood vessel centerline necessarily intersects at two points $p(\theta_{-1})$ and $p(\theta_1)$. Point $p(\theta_{-1})$ and point $p(\theta_1)$ are two ridge points adjacent to $p(\theta_0)$. Moreover, the brightness on the center line of the blood vessel is higher than that on the non-center line. Therefore, by analyzing the brightness values of all the points on the circle, the coordinates of $p(\theta_{-1})$ and $p_2(\theta_1)$ can be obtained, that is, the positions of the adjacent two ridge points.

First, the maximum value of the gray level of all the points on the circle is obtained, and the coordinates of the corresponding point $p(\theta_{\max})$ of the maximum value can be obtained, as shown in the equation (13).

$$I(p(\theta_{\max})) \ge I(p(\theta)), \quad \forall\theta \in [0, 2\pi) \tag{13}$$

Obviously, $p(\theta_{\max})$ is a point in $p(\theta_{-1})$ and $p(\theta_1)$. On the opposite direction $2\pi - \theta_{\max}$ of $\theta_{\max}$, look for another grayscale maximum point $p(\theta'_{\max})$ on the local arc length $l(2\pi - \theta_{\max} - \Delta\theta, 2\pi - \theta_{\max} + \Delta\theta)$, as shown in equation (14).

$$I(p(\theta'_{\max})) \ge I(p(\theta)), \ \forall\theta \in l(2\pi - \theta_{\max} - \Delta\theta, 2\pi - \theta_{\max} + \Delta\theta) \tag{14}$$

Obviously, $p(\theta'_{\max})$ is another point in $p(\theta_{-1})$ and $p(\theta_1)$ except $p(\theta_{\max})$, $\theta_{\max}$ and $\theta'_{\max}$ are the initial directions of forward or backward tracking.

Here, it is stipulated here that if $\cos(\theta_{\max}) \ge 0$, $\theta_{\max}$ is the direction in which p_0 is tracked forward (to the right), and $\theta'_{\max}$ is the direction in which p_0 is tracked backward (to the left). Conversely, $\theta_{\max}$ is the direction in which p_0 is tracked backwards (to the left), and $\theta'_{\max}$ is the direction in which the forward (rightward) is tracked.

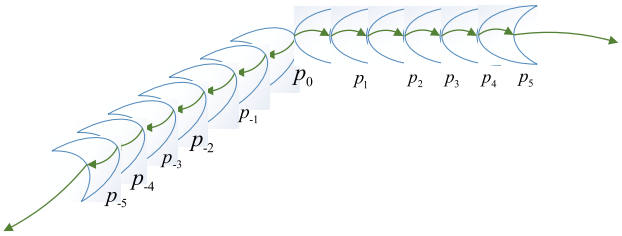

FIGURE 8. Center line tracing is formed.

C. CENTERLINE TRACKING PROCESS

In the process of tracking the ridge point, it is necessary to judge the position of the next ridge point and tracking direction according to the position and direction of the current ridge point.

The tracking method proposed in this paper can be described as follows: it is known that the current ridge position is p_1 and the tracking direction is θ_1. Set the search angle to $2\Delta\theta$ and find the gamma maximum value p_2 on the arc length $l(\theta_1 - \Delta\theta, \theta_1 + \Delta\theta)$ as shown in equation (15).

$$I(p_2) \ge I(p), \quad \forall p \in l(\theta_1 - \Delta\theta, \theta_1 + \Delta\theta) \tag{15}$$

The variable p_2 is the next ridge point obtained by the tracking. The variable θ_2 is the tracking direction used for the next tracking process. In order to track the centerline of the blood vessel, it is necessary to use the initial ridge point for forward and backward tracking.

In Figure 8, the ridge sequence $p_1, p_2, p_3, \ldots$ is obtained by tracking forward according to a certain initial ridge point p_0, and the ridge sequence $p_{-1}, p_{-2}, p_{-3}, \ldots$ is obtained by backward tracking. Connecting these ridge sequence sequences ultimately constitutes the vascular centerline structure.

There are three conditions for tracking termination during the tracking of the centerline:

1) When the detected ridge point position is outside the range of the image.

2) When the detected gradation gray level is less than a prescribed threshold.

3) When the detected ridge point and the formed center line distance are less than the specified threshold.

D. PUNCTURE OF PSEUDO VASCULAR CENTERLINE

In the process of vascular enhancement, not only the vascular portion is enhanced, but all tubular objects in the image are enhanced. After undergoing automatic tracking of the extraction centerline, the extracted centerline is not only the actual blood vessel centerline, but also the centerline of other non-vascular tubular targets, which is referred to herein as the pseudo vascular centerline. In order to get the true blood vessel centerline, these pseudo vascular centerlines need to be removed.

In human tissue, the blood vessels have a tree-like structure, and blood can reach any branch through the blood vessels, and reflected on the image, the blood vessel branches are connected. Therefore, in all the centerline sets extracted, the

vessel centerline is the largest connected branch. The center line of the blood vessel can be obtained by finding the largest connected branch, thereby eliminating other results.

Let $\{l_i\}_{i=1}^{N}$ be all N centerlines extracted and tracked in the text. The distance $d(l_i, l_j)$ between the two centerlines is represented by the shortest distance of the upper point as shown in equation (16).

$$d(l_i, l_j) = \min_{p_i \in l_i, p_j \in l_j} d(p_i, p_j) \tag{16}$$

In order to merge the connected centerlines, it is stipulated that if the distance between the two centerlines is sufficiently small, the two centerlines are considered as different branches on the same centerline. According to this principle, all centerlines are merged, and the N centerlines of $\{l_i\}_{i=1}^{N}$ are reduced to the N^* centerline in $\{l_i^*\}_{i=1}^{N^*}$.

In $\{l_i\}_{i=1}^{N}$, if $||l_i^*|| > ||l_j^*||, \forall l_j^* \in \{l_i^*\}_{i=1}^{N^*}, j \neq i$, and where $||l_i^*||$ is the number of ridge points on the connected branch l_i^*, then l_i^* is the largest connected branch, that is, the obtained true blood vessel center line.

IV. EXPERIMENTS AND RESULTS

A. DATA SET DESCRIPTION

In order to test the feasibility of the method of automatically extracting the center line of the blood vessel in the angiographic image, this paper will select the clinically acquired coronary angiography image to test it, and require the blood vessels in the image to be not only uneven in thickness, complicated in branch structure, but also in the background. There are many noises similar to the grayscale of blood vessels.

This paper collected eight sets of data for centerline extraction. Among them, the image quality of the eight sets of data sets and the number of images are shown in Table 1.

TABLE 1. Image quality of dataset.

Image Quality	Number of data sets	Number of images in the dataset
Poor	2	4000
Medium	3	6000
Good	3	6000

Each set of data was extracted from the center line of the right coronary artery (RCA), and three experiments were repeated, each using a different initial point. The original size of the data is 512 × 512 × 512, and the resolution is about $0.3 \sim 0.6$ mm ^{3}.

B. ALGORITHM ROBUSTNESS TO NOISE

In order to verify the robustness of the proposed vascular centerline extraction algorithm to noise, the following experiment was performed. Three different quality angiographic images were selected. 2000 images were selected with poor image quality. The image quality is medium and 2,000 images are selected. Select 2000 images with high image quality.

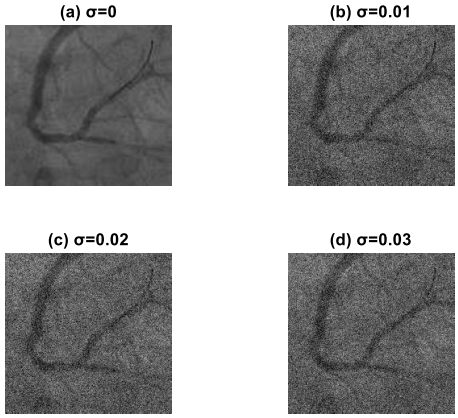

FIGURE 9. Image with noise.

Then, by adding different degrees of noise to check the sensitivity of the algorithm to noise, the added noise is Gaussian white noise, the mean is 0, and the variances are: 0.01, 0.02, and 0.03. Figure 9 shows the image after noise is added. Table 2 records the number of successful executions of the algorithm and the ratio of the total number of images in different situations.

TABLE 2. Results of algorithm execution under different noise conditions.

Image Quality	Poor	Medium	Good	Total	Percent
σ^2=0	1656	1721	1798	5175	0.863
σ^2=0.01	1601	1676	1693	4970	0.828
σ^2=0.02	1578	1581	1538	4697	0.783
σ^2=0.03	1557	1567	1512	4636	0.772

It can be seen from Table 2 that, in the absence of superimposed noise, the average success rate of the execution of the different quality image algorithms reaches 0.863, and the maximum error of the average success rate of the algorithm after the addition of noise is only 0.91. It can be concluded that the effect of noise on the result is not large, indicating that the algorithm has certain adaptability to images of different quality and is robust to noise.

This paper also tests the influence of the centerline extraction results when adding different intensity noises. Figure 10 shows the variation of the average error of the centerline extracted by the method under the condition of increasing the standard deviation of Gaussian noise. It can be seen from Figure 10 that as the noise intensity increases, the average error of the extracted center line will increase continuously to a certain extent, but both are less than 1 pixel.

C. CONTRAST IMAGE TEST RESULTS AND ALGORITHM FEASIBILITY ANALYSIS

In Figure 4, a clinical angiography image for algorithm testing has been given and the enhancement effect of the contrast

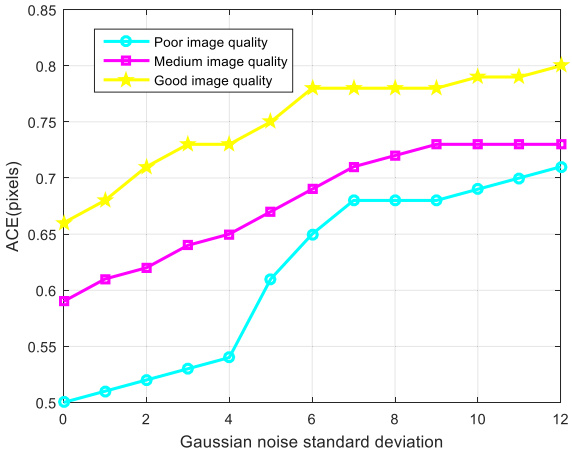

FIGURE 10. Relation between centerline extraction error and noise intensity.

FIGURE 11. A partial enlarged view of the seed point detected in the image.

image is shown. After the image is adaptively enhanced, the centerline extraction process of the blood vessel will be performed in the enhanced image as shown in Figure 4(d). In order to facilitate the contrast observation, the results will be marked in the original image.

Figure 11 shows a partial enlarged view of the detected seed points for tracking. It is not difficult to find through visual observation that the method can detect a large number of seed points, and most of them are located near the center line of blood vessels.

Figure 12(a) is a partial enlarged view showing the initial tracking directions of forward and backward at all seed points. Figure 12 (b) shows the two characteristic directions of the Hessian matrix at the seed point in the corresponding region. Through visual observation, it is not difficult to find that the method can describe the direction of the blood vessel more accurately than the method of describing the direction of the ridge point by using the characteristic direction of the Hessian matrix.

In order to compare and analyze MVEF and AMVEF, the same centerline tracking extraction and comparison are carried out for the several enhancement effects involved in Figures 4(b) ∼ 4(d), and are shown in Figure 13

(a) Local enlargement of the initial tracking direction

(b) The eigenvectors of the Hessian matrix

FIGURE 12. Detection results of initial tracking direction.

(a) Center line (β=15) (b) Center line (β=8) (c) Center line (AMVEF)

FIGURE 13. All target centerlines extracted from the enhanced image in Figure 4.

respectively. By comparison, it is found that the effect of Figure 13(c) is obviously better than that of Figure 13(a) and Figure 13(b), which not only proves the feasibility of the centerline tracking extraction method, but also shows the AMVEF relative to the superiority of MVEF.

Figure 14 is a graph showing the results of Figure 13 after rejection of the pseudo vascular centerline. Obviously, the effect of Figure 13(c) is the best. Therefore, it can be concluded that the proposed method for extracting the vascular centerline, including adaptive vascular enhancement, seed point generation, centerline tracking extraction and pseudo-vessel centerline rejection, can be fully automated in angiographic images to extract the centerline of the blood vessel.


(a) Center line (β=15) (b) Center line (β=8) (c) Center line (AMVEF)

FIGURE 14. Vascular centerline results after removal of pseudo vascular centerline.

D. ALGORITHM RESULTS AND QUANTITATIVE ANALYSIS

This paper refers to several indicators that are most widely used in vascular segmentation [34] to evaluate the method, including the accuracy and efficiency of centerline extraction in the presence of bifurcation, overlap, and noise. The specific indicators are:

(1) Overlap rate, that is, the detection rate of blood vessels, refers to the ratio of the detected centerline of the blood vessel covering the true centerline.

(2) The extraction error of the centerline can be extracted by the average error of centerline (AEC).

(3) The ratio of error of centerline extraction less than 1 pixel (REC<1) is expressed by the ratio of error of centerline extraction less than 1 pixel.

(4) The extraction amount and time of the center line.

(5) Number of seed points (NSP).

(6) Number of ridge points (NRP).

(7) Time of generation in seed points (GSP), generation of initial direction (GID), and tracking of centerline (TC).

Table 3 shows the data of the method in the quantitative analysis. It can be seen that when testing various types of images, the method can extract most of the vascular structures with coverage of overlap >0.973, and the average error distribution is about 0.5 pixels and is concentrated within 1 pixel.

E. PERFORMANCE COMPARISON WITH DIFFERENT ALGORITHMS

In order to verify the accuracy and robustness of the proposed algorithm, the experiments were compared in the literature [15], the literature [16], the literature [17], the literature [18], and the methods in this paper. Select three different image quality data sets. 2000 images were selected with poor image quality. The image quality is medium and 2,000 images are selected. Select 2000 images with high image quality. Figure 15 is a graph of experimental results for image quality of three different data sets. In this experiment, coverage was used as an evaluation index, and the results of 50 cycles were passed through five cross-validation methods.

It can be seen from the experimental data in Figure 15 that both the literature [16] and the literature [17] have certain

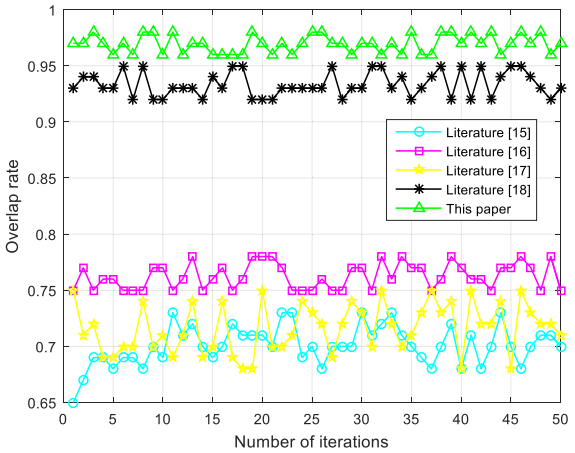

FIGURE 15. Algorithm performance comparison of data sets for different image quality.

TABLE 3. Summary of quantitative data.

Image Quality		Poor	Medium	Good
Extracting effect	NSP	125.25	97.5	120.5
	NRP	1152	906.25	1164.25
	Overlap	0.986	0.989	0.973
	AEC	0.445	0.461	0.585
	REC<1	0.974	0.967	0.923
Time consuming	GSP	1.561	1.576	1.529
	GID	0.436	0.391	0.406
	TC	2.746	1.825	2.777
	Total	4.742	3.791	4.712

limitations on the automatic extraction of the coronary centerline. Although the centerline extraction method of the literature [18] can provide complete topology information of blood vessels, it cannot automatically connect the parts of the blood vessel that are broken. Although the method of direction tracking in [19] can automatically connect the vascular disconnected parts, it cannot take into account the topological information of the whole blood vessel. Compared with the algorithm proposed in this paper, the literature [15], the literature [16], the literature [17] and the literature [18] are not robust when extracting the coronary artery centerline. This paper starts from the structural characteristics of coronary vessels. Automatic extraction of the center line of the blood vessel, the correct rate is as high as 0.989.

V. CONCLUSION

Computed tomography of coronary arteries is an important means of clinical detection of cardiovascular diseases such as coronary heart disease, and the extraction of coronary centerline is the premise of automatic analysis and detection of cardiovascular diseases. The structural extraction of blood vessels has important reference value for the diagnosis and treatment of clinical cardiovascular diseases, but the traditional extraction method requires a lot of manual intervention, which is not only time-consuming and laborious, but also brings uncertain human factors to the extraction results. In this paper, a fully automatic vascular centerline tracking extraction method is designed, including adaptive

blood vessel enhancement, initial tracking condition acquisition, automatic tracking of the centerline and rejection of the pseudo vascular centerline. In the pre-processing stage of the image, adaptive vascular enhancement of the image can highlight the structure of small-sized blood vessels and facilitate the extraction of the centerline of small branch vessels. In the extraction method of seed points, this paper performs automatic seed point detection by first-order differential and second-order differential information of images, and quickly extracts a large number of seed points located near the center line of blood vessels in the original image. When describing the tracking direction, using the zero-order information of the ridge point to replace the traditional method using the Hessian matrix eigenvector can effectively offset the error interference and be more robust. Finally, according to the connectivity characteristics of blood vessels, the blood vessel branches are combined and combined, and the largest connected branch is extracted in the result, and the pseudo-vessel center line is eliminated, and the automatic acquisition of the blood vessel center line is realized.

In addition, the method of this paper is not only suitable for two-dimensional extraction of blood vessel centerline, but also for other uses. The automatic acquisition method of tracking seed points as proposed in the paper can be used for other segmentation methods that need to set initial seed points, such as segmentation methods for region growth. If the method is extended, the conditions on the line, face, and circle are extended to the conditions of face, body, and ball respectively, and the expansion from 2D to 3D can be completed to realize the automatic tracking and extraction of the three-dimensional blood vessel center line.

REFERENCES

[1] Y. Li, X. Xie, and H. Zhang, "Image quality and impact factors for single heart-beat coronary CTA using prospectively ECG-triggered 256-slice CT," *Chin. J. Interventional Imag. Therapy*, vol. 15, no. 6, pp. 369–373, 2018.

[2] W. J. Liu, G. Z. Li, H. F. Liu, and J. Q. Lei, "Diagnostic accuracy of dual-source computed tomography angiography for the detection of coronary in-stent restenosis: A systematic review and meta-analysis," *Echocardiography*, vol. 35, no. 2, pp. 541–550, 2018.

[3] X. F. Zhang, D. Y. Hu, and R. J. Ding, "Status and trend of cardio-cerebral-vascular diseases mortality in China: Data from national disease surveillance system between 2004 and 2008," *Zhonghua Xin Xue Guan Bing Za Zhi*, vol. 40, no. 3, pp. 179–187, Mar. 2012.

[4] Y. Shimizu, S. Sato, J. Koyamatsu, H. Yamanashi, M. Nagayoshi, K. Kadota, S.-Y. Kawashiri, and T. Maeda, "Possible mechanism underlying the association between height and vascular remodeling in elderly Japanese men," *Oncotarget*, vol. 9, no. 8, pp. 7749–7757, Dec. 2018.

[5] S. Balocco, C. Gatta, F. Ciompi, A. Wahle, P. Radeva, S. Carlier, G. Unal, E. Sanidas, J. Mauri, X. Carillo, T. Kovarnik, C. W. Wang, H. C. Chen, T. P. Exarchos, D. I. Fotiadis, F. Destrempes, G. Cloutier, O. Pujol, M. Alberti, E. G. Mendizabal-Ruiz, M. Rivera, T. Aksoy, R. W. Downe, and I. A. Kakadiaris "Standardized evaluation methodology and reference database for evaluating IVUS image segmentation," *Comput. Med. Imag. Graph.*, vol. 38, no. 2, pp. 70–90, 2014.

[6] G. Robertson, E. Pellegrini, C. Gray, E. Trucco, and T. MacGillivray, "Investigating post-processing of scanning laser ophthalmoscope images for unsupervised retinal blood vessel detection," in *Proc. IEEE Symp. Comput. Based Med. Syst.*, Jun. 2013, vol. 8271, no. 1, pp. 441–444.

[7] A. P. Tagliari, A. N. Kochi, and L. E. P. Rohde, "Spontaneous left anterior descending coronary artery dissection requiring coronary artery bypass surgery," *Brazilian J. Cardiovascular Surg.*, vol. 32, no. 6, pp. 536–538, Dec. 2017.

[8] S. R. Fleagle, M. R. Johnson, C. J. Wilbricht, D. J. Skorton, R. F. Wilson, C. W. White, M. L. Marcus, and S. M. Collins, "Automated analysis of coronary arterial morphology in cineangiograms: Geometric and physiologic validation in humans," *IEEE Trans. Med. Imag.*, vol. 8, no. 4, pp. 387–400, Dec. 1989.

[9] B. Pathak and B. R. Boruah, "Improvement in error propagation in the Shack–Hartmann-type zonal wavefront sensors," *J. Opt. Soc. Amer. A, Opt. Image Sci.*, vol. 34, no. 12, pp. 2194–2202. 2017.

[10] X. Qiao, J. Bao, L. Zeng, J. Zou, and D. Li, "An automatic active contour method for sea cucumber segmentation in natural underwater environments," *Comput. Electron. Agricult.*, 135, pp. 134–142, Apr. 2017.

[11] Y.-Z. Zeng, Y. Q. Zhao, and P. Tang, "Liver vessel segmentation and identification based on oriented flux symmetry and graph cuts," *Comput. Methods Programs Biomed.*, vol. 150, pp. 31–39, Oct. 2017.

[12] V. I. Pudov and Y. N. Dragoshanskii, "Formation of the magnetic domain structure and properties of magnetic cores under conditions of ordered laser deformations," *Doklady Phys.*, vol. 62, no. 9, pp. 411–414, Sep. 2017.

[13] D. Breitenreicher, M. Sofka, S. Britzen, and S. K. Zhou, "Hierarchical discriminative framework for detecting tubular structures in 3D images," in *Information Processing in Medical Imaging*, vol. 23. Berlin, Germany: Springer, 2013, pp. 328–339.

[14] M. Bayat, M. Fatemi, and A. Alizad, "Background removal and vessel filtering of noncontrast ultrasound images of microvasculature," *IEEE Trans. Biomed. Eng.*, vol. 66, no. 3, pp. 831–842, Mar. 2019.

[15] Y. Cao, Z. Wang, L. Shen, X. Xiao, and L. Yang, "Fusion of pixel-based and object-based features for road centerline extraction from high-resolution satellite imagery," *Acta Geodaetica Cartogr. Sinica*, vol. 45, no. 10, pp. 1231–1240, 2016.

[16] G. V. Shrichandran, S. Sathiyamoorthy, P. D. Malarchelvi, and S. Kezia, "A hybrid glow-worm swarm optimization with bat algorithm based retinal blood vessel segmentation," *J. Comput. Theor. Nanosci.*, vol. 14, no. 6, pp. 2601–2611, Nov. 2017.

[17] S. P. Rajan and V. Kavitha, "Diagnosis of cardiovascular diseases using retinal images through vessel segmentation graph," *Current Med. Imag. Rev.*, vol. 13, no. 4, pp. 454–459, Nov. 2017.

[18] G. W. Alam, E. Pihan, B. Marie, and N. Mangelinck-Noël, "Impact of the seed layer morphology on the initial growth of HPMC-Si ingot," *Phys. Status Solidi*, vol. 14, no. 10, Oct. 2017, Art. no. 1700177.

[19] E. Bayam, M. Kahyaoğlu, A. Güner, R. Zehir, and C. Y. Karabay, "Safe entry site for coronary angiography: Snuff box," *Turk Kardiyol Dern Ars*, vol. 46, no. 3, pp. 228–230, Apr. 2018.

[20] M. Rashid, D. L. Fischman, S. C. Martinez, Q. Capers, M. Savage, A. Zaman, N. Curzen, J. Ensor, J. Potts, M. Mohamed, C. S. Kwok, T. Kinnaird, R. Bagur, and M. Mamas, "Temporal trends and predictors of time to coronary angiography following non-ST-elevation acute coronary syndrome in the USA," *Coronary Artery Disease*, vol. 30, no. 3, pp. 159–170, May 2019.

[21] D. A. Scaduto, O. Tousignant, and W. Zhao, "Experimental characterization of a direct conversion amorphous selenium detector with thicker conversion layer for dual-energy contrast-enhanced breast imaging," *Med. Phys.*, vol. 44, no. 8, pp. 3965–3977, Aug. 2017.

[22] K. W. Lipsø, E. S. S. Hansen, R. S. Tougaard, C. Laustsen, and J. H. Ardenkjær-Larsen, "Dynamic coronary MR angiography in a pig model with hyperpolarized water," *Magn. Reson. Med.*, vol. 80, no. 3, pp. 1165–1169, Sep. 2018.

[23] S.-Z. Chen, Z. Wang, S. S. Yu, G. Zhang, and Y. Zhang "A novel alternative to traditional *n* HSLC: An *n*-Switched-Cell based approach to high-step-up converters," *IEEE Access*, vol. 7, pp. 114529–114538, 2019.

[24] J. Wang, G. Wen, Z. Duan, and J. Lu, "Stochastic consensus control integrated with performance improvement: A consensus-region based approach," *IEEE Trans. Ind. Electron.*, to be published.

[25] N. Luo and Q. Wang, "Effective outlier matches pruning algorithm for rigid pairwise point cloud registration using distance disparity matrix," *IET Comput. Vis.*, vol. 12, no. 2, pp. 220–232, Sep. 2018.

[26] Z. Huang, Y. He, Y. Wen, and X. Song, "Injured probability assessment in frontal pedestrian-vehicle collision counting uncertainties in pedestrian movement," *Saf. Sci.*, vol. 106, pp. 162–169, Jul. 2018.

[27] J.-H. Jang and K.-S. Hong, "Linear band detection based on the Euclidean distance transform and a new line segment extraction method," *Pattern Recognit.*, vol. 34, no. 9, pp. 1751–1764, Sep. 2001.

[28] D. Kularatne, S. Bhattacharya, and M. Ani Hsieh, "Going with the flow: A graph based approach to optimal path planning in general flows," *Auton. Robots*, vol. 42, no. 3, pp. 1–19, Oct. 2018.

[29] Y. Liu, Q. Wang, H. Hu, and Y. He, "A novel real-time moving target tracking and path planning system for a quadrotor UAV in unknown unstructured outdoor scenes," *IEEE Trans. Syst., Man, Cybern. Syst.*, vol. 49, no. 11, pp. 2362–2372, Nov. 2019.
[30] L. Taotao, Y. Feng, and L. Shigeng, "Extraction method of line-structured light stripe center based on gauss-lorenz decomposition peak fitting," *Laser Optoelectron. Prog.*, vol. 56, no. 7, 2019, Art. no. 071201.
[31] M. N. Andrianov, V. I. Kostenko, and S. F. Likhachev, "Tropospheric effect on the transmissivity of the spacecraft–ground tracking station communication line," *Cosmic Res.*, vol. 57, no. 4, pp. 261–265, Jul. 2019.
[32] J. Wu, S. Yang, and Z. Xiao, "Measurement of arteriolar-to-venular diameter ratio based on hessian matrix and multi-scale analysis," *J. Med. Imag. Health Inform.*, vol. 8, no. 1, pp. 38–44, Jan. 2018.
[33] G. L. Causer, D. L. Cortie H. Zhu, M. Ionescu, G. J. Mankey, X. L. Wang, and F. Klose, "Direct measurement of the intrinsic sharpness of magnetic interfaces formed by chemical disorder using a He^{+} beam," *Acs Appl. Mater. Interfaces*, vol. 10, no. 18, pp. 16216–16224, 2018.
[34] Y. Zhiyong, X. Hongxu, L. Yuze, J. Haisong, and J. Shan, "Research on key technologies of pulmonary vascular trees segmentation based on thoracic CT images," *Tianjin Daxue Xuebao*, vol. 51, no. 2, pp. 175–180, 2018.

XIAODONG SHENG is currently the Associate Director of the Changshu No.2 People's Hospital, China, where he is also the Chief Physician with the Department of Cardiology. His research area includes machine learning and its applications on medicine.

TAO FAN is currently a Doctor with the Department of Cardiology, Changshu No.2 People's Hospital. His research area includes machine learning and its applications on medicine.

XIAOQI JIN is currently a Doctor with the Department of Cardiology, Changshu No.2 People's Hospital. His research area includes machine learning and its applications on medicine.

JING JIN is currently a Doctor with the Department of Cardiology, Changshu No.2 People's Hospital. Her research area includes artificial intelligent and its applications on medicine.

ZHIXIAN CHEN is currently a Doctor with the Department of Cardiology, Changshu No.2 People's Hospital. His research area includes artificial intelligent and its applications on medicine.

GUANQUN ZHENG is currently a Doctor with the Department of Cardiology, Changshu No.2 People's Hospital. His research area includes artificial intelligent and its applications on medicine.

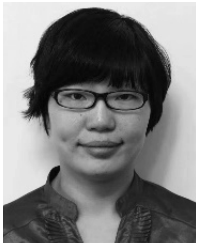

MIN LU is currently a Doctor with the Department of Cardiology, Changshu No.2 People's Hospital. Her research area includes artificial intelligent and its applications on medicine.

ZONGCHENG ZHU is currently a Doctor with the Department of Cardiology, Changshu No.2 People's Hospital. His research area includes artificial intelligent and its applications on medicine.